applied sciences

MDPI

Article

Materials Optimization and Service Performance Evaluation of a Novel Steel Bridge Deck Pavement Structure: A Case Study

Yu Haibara [1], Hanbin Ge [1] and Jia Sun [2,*]

[1] Department of Civil Engineering, Meijo University, Nagoya 468-8502, Japan; 213443501@ccmailg.meijo-u.ac.jp (Y.H.); gehanbin@meijo-u.ac.jp (H.G.)
[2] School of Transportation, Southeast University, Nanjing 211189, China
* Correspondence: sunjia_0223@163.com

Abstract: Although the double-layer pavement structure with a top layer of stone mastic asphalt concrete (SMAC) and a bottom layer of epoxy asphalt concrete (EAC) has been confirmed to have excellent overall performance in the laboratory, there is a lack of comparison and verification in practical projects. Hence, the utilization of the SMAC + EAC structure in this steel bridge deck pavement (SBDP) practical project and the clarification of its service performance are of significant importance for facilitating the promotion and application of this novel structure. This study relied on an SBDP reconstruction project in Ningbo, China. Indoor performance tests were used to determine the appropriate material compositions for SMAC and EAC. Subsequently, both ERS and SMAC + EAC pavement structures were paved in the project, and the service conditions of the different pavements after one year of operation were tested and compared. The results indicated that the epoxy SBS asphalt (ESA) binder prepared by substituting SBS-modified asphalt binder for the base binder, exhibited improved mechanical strength and toughness. The variation of modifier content significantly affected the high-temperature stability, low-temperature crack resistance, and moisture damage resistance of epoxy SBS asphalt concrete (ESAC) and high-viscosity SBS asphalt concrete (HSAC), while the gradation mainly influenced the skid resistance. The optimal contents of modifiers in ESA and HAS binders were finalized at 45 wt% and 11 wt%. After one year of operation on the trial road, the pavement performance of the SMAC + EAC structure had significant advantages over the ERS system, with all lanes having an SBDP quality index (SDPQI) above 90 and an excellent service condition. The successful application of the SMAC + EAC structure validated its applicability and feasibility in SBDP, which provided strong evidence for the further promotion of this structure.

Keywords: steel bridge deck pavement; SMAC + EAC; material optimization; performance evaluation; case study

Citation: Haibara, Y.; Ge, H.; Sun, J. Materials Optimization and Service Performance Evaluation of a Novel Steel Bridge Deck Pavement Structure: A Case Study. *Appl. Sci.* **2023**, *13*, 5930. https://doi.org/10.3390/app13105930

Academic Editor: Victor Franco Correia

Received: 18 April 2023
Revised: 7 May 2023
Accepted: 9 May 2023
Published: 11 May 2023

1. Introduction

The rapid development of transportation infrastructure plays a vital role in higher economic growth. As an essential part of road engineering, bridges are of great significance in improving traffic fluidity and travel convenience [1,2]. Numerous large-span bridges have been designed and constructed in riverside and coastal areas. The orthotropic steel bridge decks have been widely used due to the advantages of light-weight, high-strength, and easy construction [3]. As the control node of highway transportation, the traffic volume and heavy vehicle proportion of the bridge are much higher than those of ordinary roads. The overload phenomenon frequently occurs, leading to higher requirements for steel bridge deck pavement (SBDP) performance on materials [4]. Studies and practices revealed that epoxy asphalt concrete (EAC), guss asphalt concrete (GAC), and modified stone mastic asphalt concrete (SMAC) were more widely used materials for SBDP [5,6].

Initially, these materials were introduced into China as single-layer structures. Due to the lack of consideration of environmental variability and the effects of vehicle loads, the

pavement suffered severe damage within a short service period [7]. To this end, considering that single-layer pavement structures had difficulty meeting the utilization requirements of bridges, the double-layer pavement structure gradually attracted the attention of researchers. In contrast, double-layered pavement structures can be designed separately and fully integrate the advantages of different materials [8,9]. After years of research and attempts, EAC + EAC, SMAC + SMAC, and SMAC + GAC are the most commonly used double-layer SBDP structures [10–12]. Undoubtedly, epoxy asphalt (EA) is a thermosetting material, and the EAC prepared using EA has excellent comprehensive performance, which enables the successful application of the double-layer EAC structure in SBDP [13,14]. However, the structure has stringent requirements for construction conditions, and the high price limits its further promotion [15]. The double-layer SMAC structure has good skid resistance and water stability and benefits from a short construction period and low cost. However, the structure has insufficient high-temperature stability and was prone to rutting disease in hot summers [16]. SMAC + GAC is a double-layer heterogeneous pavement structure that fully utilizes the superiority of both SMAC and GAC. The GAC in the lower layer has good toughness and waterproof properties and synergizes well with the steel bridge plate, while the SMAC in the upper layer is used as a wearing layer due to its satisfactory anti-skid properties. Unfortunately, the SMAC + GAC structure is prone to rutting, potholes, and other defects under continuous high-temperature conditions [17,18]. Recently, an ERS pavement system consisting of an epoxy bonding chip layer (ECBL), resin asphalt concrete (RAC), and SMAC has been proposed to maximize the characteristics of various materials and to ensure that the deck has good service performance and traffic safety. However, the structure has proven to suffer from frequent rutting defects under the coupled effects of high temperature and heavy loads. However, the damage, such as displacement and upheaval caused by insufficient shear strength between SMAC and RAC, cannot be ignored [19,20].

It is known that all of the above double-layer SBDP structures have deficiencies. In this case, it is necessary to investigate and attempt a novel SBDP structure. The structure of SMAC + EAC has been revealed to be of great research value [13]. Luo et al. tested and evaluated the performance of four double-layer pavement structures, such as EA–GA, SMA–GA, SMA–EA, and EA–EA. The results indicated that although the SMA–EA structure did not have the best performance in all categories, the structure had good overall performance, and fatigue damage occurred in the top layer of SMAC, which was easy to repair and maintain [8]. Chen et al. presented the long-life steel bridge deck pavement (LLSBDP) and proposed the "SMA + EAC" pavement structure. The material and structural performance of SMA + EAC was evaluated by combining numerical analysis and indoor tests and compared with the double-layer EAC structure. The results demonstrated that the pavement material had good stability and deformation coordination with the steel bridge panels. Moreover, it was difficult to extend the defects of the SMA layer to the EAC layer, and only the top SMA layer needed to be repaired or reconstructed periodically, extending the service life of the SBDP. Additionally, the better skid resistance and lower cost of SMA gave the structure significant economic and social benefits [21]. Sun et al. optimized the pavement materials for the SMAM + EAM structure and compared and analyzed the dynamic mechanical response of different pavement structures using finite element analysis. From the results, it can be seen that the performance of the SMAM + EAM structure could meet the application requirements of the SBDP. Compared with double-layer EAM, although the deformation resistance of the SMAM + EAM structure was reduced, the low-temperature crack resistance and interlayer shear resistance were improved [22]. The above research indicates that the SMAC + EAC structure can fully utilize the advantages of both materials and has application and promotion potential. Specifically, with excellent overall performance, EAC is used in the bottom layer as a waterproof and load-bearing layer to protect the steel bridge plate whilst providing coordinated deformation capability; SMAC in the top layer is used as a wearing layer to ensure driving safety. Additionally, only the top layer of SMAC needs to be repaired or resurfaced when the pave-

ment layer is severely damaged, which has the advantage of being easy to maintain with a low cost. Notably, although scholars have conducted many indoor tests and simulations on SMAC + EAC structures, there is a lack of comparison and verification of entity projects.

On this basis, this study based on the SBDP reconstruction project of the Chuanshan-Ningbo highway, the ERS system and SMAC + EAC structure were adopted on the lanes on two sides, respectively, and the comparative evaluation was carried out in combination with the operation. This study aims to verify the excellent overall performance and feasibility of the SMAC + EAC structure through entity engineering and promote the scaled application of this structure in SBDP. Firstly, tensile and viscosity tests were used to evaluate the mechanical properties and construction allowable time of epoxy SBS asphalt (ESA) binders with different epoxy resin (EP) contents. Then, the mixtures prepared with different ESA binders and high-viscosity SBS asphalt (HSA) binders were analyzed for high-temperature stability, low-temperature crack resistance, moisture damage resistance, and skid resistance, and the appropriate modifier contents were selected by considering performance and cost. Finally, the trial road lanes that have been in operation for one year were tested to compare and evaluate the service conditions of the ERS and SMAC + EAC structures.

2. Background of the Trial Road

This trial road is located in Ningbo City, Zhejiang Province, China. It is a part of the Chuanshan–Ningbo highway, as shown in Figure 1. The bridge is a steel box girder bridge with a span of 40 + 65 + 50 m in the Chuanshan direction and 50 + 65 + 40 m in the Ningbo direction. The previous bridge deck pavement was the ERS system, specifically SMA-10 (3 + 3 cm) + RA-05 (2 cm). However, the bridge deck pavement suffered from rutting and potholes after four years of operation and deteriorated rapidly thereafter, with significant deterioration in the service quality. To this end, the previous pavement was milled and resurfaced. Among them, the deck pavement in the Chuanshan direction continued to utilize the ERS system, as shown in Figure 2a; a novel deck pavement structure was adopted in the Ningbo direction, and the new structure maintained the same pavement thickness (8 cm). According to the previous research results, the specific scheme was determined as SMA-13 (4.5 cm, high-viscosity SBS asphalt concrete) for the upper layer and EA-10 (3.5 cm, epoxy SBS asphalt concrete) for the lower layer [22], as shown in Figure 2b.

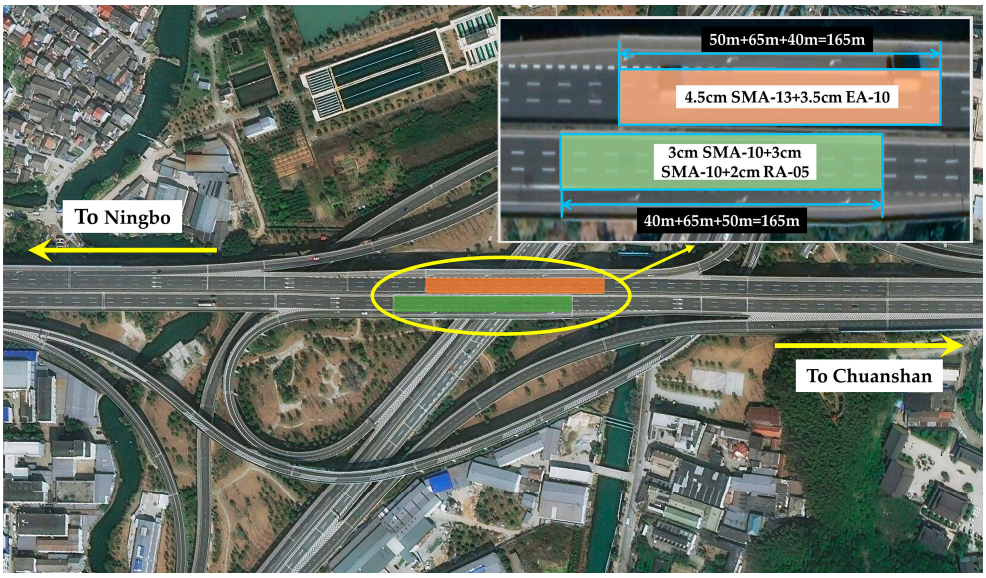

Figure 1. Location and basic information of the trial road.

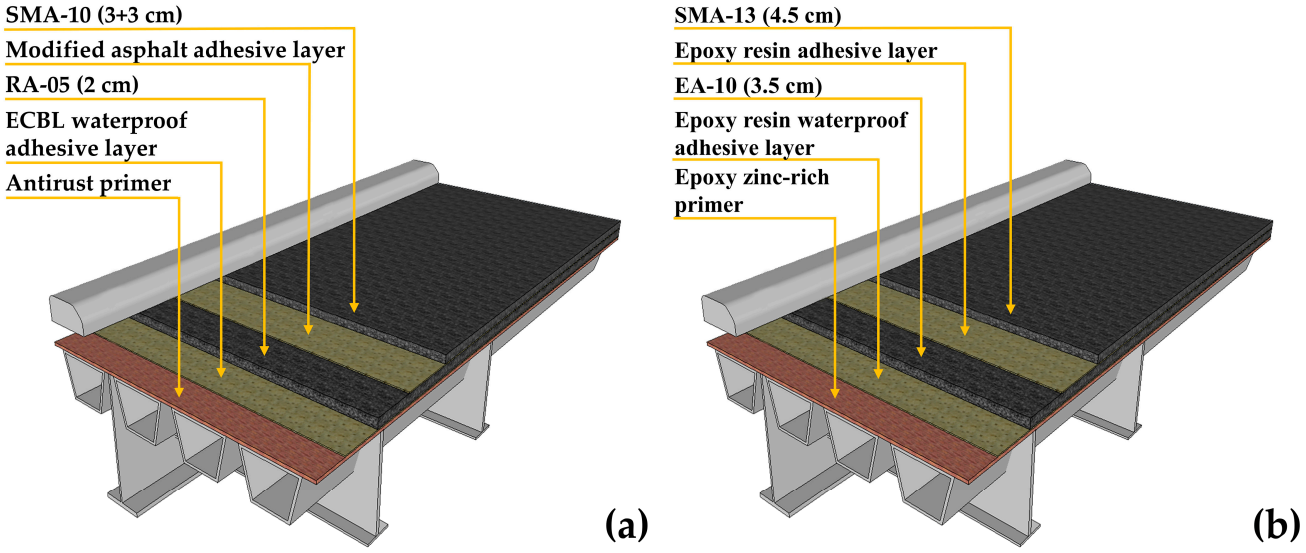

Figure 2. Steel bridge deck resurfacing scheme: (**a**) Chuanshan direction; (**b**) Ningbo direction.

3. Materials and Methods

3.1. Raw Materials

The raw materials used in this study include SBS (I-D) modified asphalt binder with a linear SBS content of 4.5 wt% (China Petroleum & Chemical Corporation Zhenhai Refining & Chemical Branch, Ningbo, China), KD-BEP epoxy resin and curing agent (KINDAI KASEI Co., Ltd., Osaka, Japan), TAFPACK-Super (TPS) (Taiyo Construction Co., Ltd., Nagoya, Japan) and lignin fibers (Guangzhou Shenchuang Chemical Co., Ltd., Guangzhou, China). Moreover, the aggregates used to prepare asphalt concrete consisted of coarse basalt aggregate, fine basalt aggregate, and limestone mineral powder, which were supplied by Zhenjiang Maodi Industrial Co., Ltd. (Zhenjiang, China). The properties of the raw materials satisfied the "Technical specification for the construction of highway asphalt pavements" (JTG F40-2004) and the "Specifications for Design and Construction of Pavement on Highway Steel Deck Bridge" (JTG/T3364-02-2019) [23,24]. The basic properties of SBS-modified asphalt binder and modifiers are shown in Tables 1 and 2.

Table 1. Basic properties of SBS (I-D) modified asphalt binder.

Technical Index		Unit	Result	Specification
Penetration (25 °C, 100 g, 5 s)		0.1 mm	54.4	40–60
Ductility (5 cm/min, 5 °C)		cm	34	≥30
Softening point		°C	80.5	≥80
Penetration index		/	0.76	≥0
Dynamic viscosity (135 °C)		Pa·s	2.57	≤3.0
Flash point		°C	291	≥230
Elastic restitution (25 °C)		%	88	≥80
Solubility		%	99.5	≥99
Density (15 °C)		g/cm^3	1.021	/
RTFOT (163 °C, 5 h)	Mass loss	%	−0.16	≤±1.0
	Penetration ratio	%	76	≥65
	Ductility (5 °C, 5 cm/min)	cm	23	≥20

Table 2. Basic properties of modifiers.

Modifier Type	Basic Performance
Epoxy resin	Viscosity (23 °C): 3090 mPa·s; relative density (23 °C): 1.12; appearance: light yellow liquid
Curing agent	Viscosity (23 °C): mPa·s; relative density (23 °C): 0.89; appearance: transparent liquid
TPS	Melt index: 3.1 g/10 min; size: 4.2 mm
Lignin fiber	Fiber length: 6.6 mm; ash content: 17.1%; oil absorption rate: 6.1 times of fiber mass; moisture content: 2.9%

3.2. Mixing Parameters

It has been shown that when the EP content reaches 35 wt%, the EP phase in the EA binder undergoes a phase transition with the asphalt phase, and the binder changes from a thermoplastic to a thermosetting material [25]. Additionally, considering that the EP content of the EA binder commonly used in current engineering was 50 wt% [26,27], the EP content in the ESA binder was determined to be 35, 40, 45, and 50 wt% and designated as ESA35, ESA40, ESA45, and ESA50. ESACs prepared with the above ESA binders were labeled ESAC35, ESAC40, ESAC45, and ESAC50, respectively. TPS is mainly composed of thermoplastic rubber, which can absorb the lighter components of asphalt when it swells at high temperatures, increasing the viscosity of the binder and improving its comprehensive properties [28]. Currently, the additive amount of TPS in SBS-modified asphalt binder is generally 8–12 wt% [29,30]. Hence, the TPS content in the HSA binder was set to 7, 9, 11, and 13 wt%, and the HSACs prepared were labeled as HSAC7, HSAC9, HSAC11, and HSAC13, respectively. Additionally, the amount of lignin fiber added to the concrete was 0.3 wt% of the aggregates.

3.3. Mixture Preparation and Design

The preparation procedures of the ESA binder are as follows: (i) the KD-BEP epoxy resin and curing agent were preheated to 60 °C, and the SBS-modified asphalt binder was preheated to 170 °C; (ii) epoxy resin and curing agent were mixed in the mass ratio of 56:44, with stirring conditions of 500 rpm and 60 °C/3 min; (iii) the epoxy blend was added to SBS-modified asphalt binder. The stirring conditions were 500 rpm and 170 °C/3 min to obtain the ESA binder.

The preparation procedures of the HSA binder were as follows: (i) the SBS-modified asphalt binder was preheated to 170 °C in advance; (ii) TPS and SBS-modified asphalt binder were mixed in accordance with the specified mass ratio, using a shear rate, temperature and time of 5000 rpm, 170 °C and 30 min, respectively, to obtain the HSA binder.

The ESAC and HSAC were prepared as follows: (i) the aggregates were preheated to 170 °C in advance; (ii) the coarse and fine aggregates were poured into the mixing pot at 170 °C. For HSAC, a quantitative amount of lignin fibers were also poured, followed by stirring for 75 s; (iii) the prepared asphalt binder was poured into the mixing pot and stirred for 75 s; (iv) the mineral powder was poured and stirring was continued for 75 s under the same conditions to obtain asphalt concrete. Notably, the ESAC should be placed in an oven to regenerate at 60 °C for 4 d.

According to the Chinese specifications (JTG F40-2004) and (JTG/T3364-02-2019) [23,24], the gradation used for the top and bottom layers were SMA-13 and EA-10, respectively, and their synthetic gradation results are shown in Figure 3. The optimum asphalt–aggregate ratios for HSAC and ESAC were determined to be 6.2% and 6.5%, respectively.

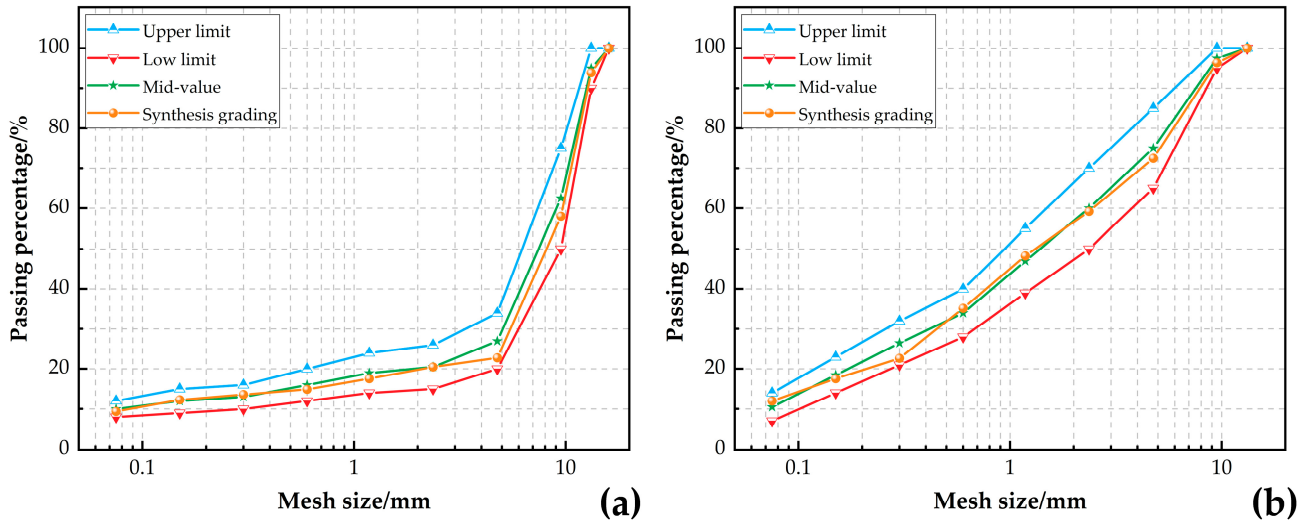

Figure 3. Gradation design results for the asphalt concrete: (**a**) SMA-13 and (**b**) EA-10.

4. Test and Evaluation Methods

For ASTM D638 and ASTM D4402, the mechanical properties and construction allowable time of the ESA binder were evaluated [31,32]. According to "Standard Test Methods of Bitumen and Bituminous Mixtures for Highway Engineering." (JTG E20-2011) and "Field Test Methods of Highway Subgrade and Pavement" (JTG 3450-2019) [33,34], the rutting test, beam bending test, water immersion Marshall test, freeze–thaw splitting test, and pendulum friction test were conducted. The high-temperature rutting resistance, low-temperature cracking resistance, moisture damage resistance, and skid resistance of ESAC and HSAC were analyzed. The detailed concrete test information, specification requirement values, and evaluation index calculation methods are shown in Tables 3 and 4. Additionally, with reference to "Technical Specification for Maintenance Technology of Long Span Bridge Steel Deck Epoxy Asphalt Concrete Pavement" (DB32/T 3292-2017) and "Highway Performance Assessment Standards" (JTG 5210-2018) [35,36], the pavement performance of the trial road after one year of operation was tested and evaluated.

Table 3. Basic information on concrete performance tests.

Test	Specimen Size/mm	Evaluation Index	Test Temperature/°C	Specification	Test Standard
Rutting test	300 × 300 × 50	Dynamic stability (*DS*)	70	≥6000 times/mm	T0719-2011
Beam bending test	250 × 30 × 35	Maximum flexural strain (ε_B)	−10	≥3000 με	T0715-2011
Immersion Marshall test	Φ101.6 × 63.5	Residual stability (*RS*)	23	≥85%	T0709-2011
Freeze–thaw splitting tensile strength test	Φ101.6 × 63.5	Tensile strength ratio (*TSR*)	23	≥80%	T0729-2011
Pendulum test	300 × 300 × 50	British pendulum number (*BPN*)	20	≥45	T0964-2008

4.1. Laboratory Binder Performance Test

The tensile tests were performed on ESA35, ESA40, ESA45, and ESA50 binders using the WDW-100 universal material tensile machine manufactured by Jinan Fangyuan Testing Instruments Co., Ltd. (Jinan, China), and the tensile strength (*TS*) and elongation at break (*EB*) of the specimens were calculated. The test rate and temperature were 500 mm/min and 23 °C, respectively. For the same binder, at least three parallel tests were performed.

Table 4. Equations for evaluation indexes.

Evaluation Index	Calculation Equation	Symbol Explanation	Equation Number
DS	$DS = \frac{(t_2 - t_1) \times N}{d_2 - d_1} \times C_1 \times C_2$	d_1: the deformation corresponding to t1 (45 min), mm; d_2: the deformation corresponding to t2 (60 min), mm; C_1: the correction factor for the type of testing machine; C_2: the coefficient of the specimen; N: the round-trip speed of the test wheel, 42 times/min.	(1)
ε_B	$\varepsilon_B = \frac{6 \times h \times d}{L^2}$	h: the height of the specimen, mm; L: the span of the specimen, mm; d: the specimen deflection at the time of damage, mm.	(2)
RS	$RS = \frac{MS_2}{MS_1} \times 100$	MS_2: Marshall stability of specimens after 48 h of soaking; MS_1: Marshall stability of specimens after 45 min of soaking.	(3)
TSR	$TSR = \frac{RT_2}{RT_1} \times 100$	RT_2: the splitting strength of specimens after freezing and thawing, MPa; RT_1: the splitting strength of specimens without freezing and thawing, MPa.	(4)

The NDJ-1C asphalt Brinell viscometer manufactured by Shanghai Meiyu Testing Instruments Co., Ltd. (Shanghai, China) was used to conduct viscosity tests on ESA35, ESA40, ESA45, and ESA50 binders. The 27# rotor and 50 r/min rotational speed were selected, and the test temperature was 170 °C to fit the actual construction.

4.2. Laboratory Concrete Performance Test

The rutting test was carried out using an HYCZ-5 automatic rutting tester manufactured by Hebei Kebiao Testing Instruments Co., Ltd. (Cangzhou, China). The rutting test specimens with a size of 300 × 300 × 50 mm were prepared, in which ESAC was cured at 60 °C for 4 d; the specimens were placed on the test bench together with the test mold, and the tester was started so that the test wheel traveled back and forth at 70 °C for 60 min; the high-temperature stability of the concrete was evaluated using the dynamic stability (*DS*) calculated according to Equation (1).

The beam bending test was carried out using a UTM-25 multifunctional material testing machine that IPC Global (Melbourne, Australia) manufactured. The slab-shaped specimens were cut into prismatic specimens of 250 × 30 × 35 mm and placed in a constant temperature chamber at −10 °C for not less than 45 min; the specimens were then removed and placed on the instrument bracket, and the temperature and loading rate of the test were −10 °C and 50 mm/min, respectively; the maximum bending tensile strain (ε_B) at the bottom of the specimens was calculated using Equation (2).

The specimens were formed using a SMDJ-1 Marshall compaction instrument manufactured by Shanghai Shenrui Testing Equipment Manufacturing Co., Ltd. (Shanghai, China) with dimensions of Φ101.6 × 63.5 mm, of which ESAC needs to be cured at 60 °C for 4 d. For the water immersion Marshall test, the identical specimens were divided into two groups and placed in a constant temperature water bath, with one group holding a condition of 60 °C/48 h, while the other group was 60 °C/45 min; the specimens were tested using an LWD-6 Marshall Stability Instrument (Cangzhou, China) produced by Cangzhou Yixuan Testing Instruments Co., Ltd. and the residual stability (*RS*) was calculated according to Equation (3).

The specimens were separated into two groups for the freeze–thaw splitting test, and one group was stored at room temperature. The other group was kept under a vacuum of 97.3~98.7 kPa (730~740 mmHg) for 15 min and then placed in water for 30 min after restoring normal pressure; subsequently, the specimens were taken out and put into plastic bags, and about 10 mL of water was added and placed into a constant temperature

refrigerator at −18 °C for 16 h; then, the plastic bags were withdrawn, and the specimens were taken out and placed into a constant temperature water bath at 60 °C for 24 h; finally, the two groups of specimens were placed into the constant temperature sink at 25 °C for 2 h. The splitting test was executed on two groups of specimens with the temperature and loading rate of 23 °C and 50 mm/min, respectively, and the tensile strength ratio (*TSR*) was calculated using Equation (4).

A BM-3 pendulum friction coefficient tester manufactured by Tianjin Jiansong Instrument Technology Ltd. (Tianjin, China) was adopted. The surface of the specimen was cleaned, and the instrument calibrated. Before the test, an appropriate amount of water was sprayed on the specimen surface and kept moist, followed by testing the specimen, and the test temperature was 20 °C.

It should be noted that at least three parallel specimens were used in all of the above concrete performance tests.

4.3. Service Performance Evaluation

As shown in Figure 4, K0008+800 was taken as the dividing line for the comprehensive inspection of the bridge deck pavement conditions at K0008+700 to K0008+800 (right) and K0008+800 to K0008+900 (left). The three lanes in the Ningbo direction were named NB1, NB2, and NB3, and the three lanes in the Chuanshan direction were designated CS1, CS2, and CS3. The inspection included the SBDP condition index (SDPCI), SBDP riding quality index (SDRQI), SBDP rutting depth index (SDRDI), and SBDP wearing index (SDPWI). The comprehensive condition was assessed using the SBDP quality index (SDPQI), which was weighted by four sub-indices, SDRDI, SDRQI, SDPCI, and SDPWI, as shown in Equation (5).

$$SDPQI = (0.35SDPCI + 0.3SDRQI + 0.15SDPCI + 0.1SDPCI)/0.9 \quad (5)$$

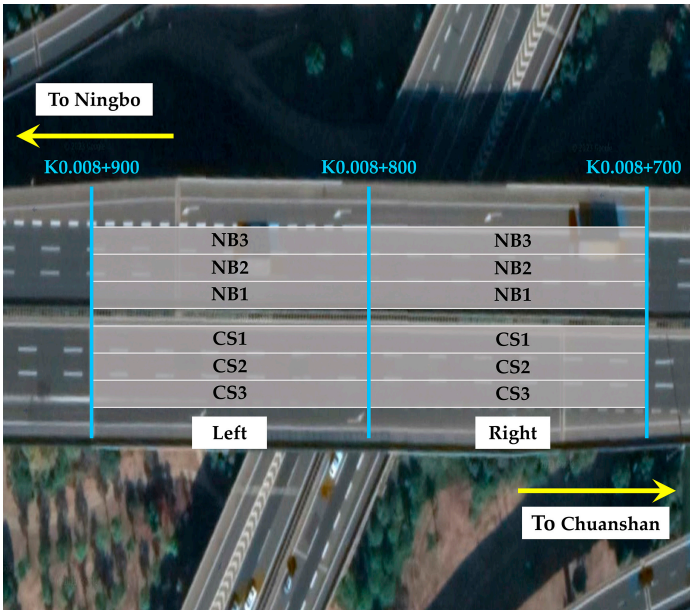

Figure 4. Designation of trial road lanes.

5. Results and Discussion

5.1. Mechanical Property and Viscosity Characteristics of the ESA Binder

The tensile test results for different ESA binders are shown in Figure 5a. As the EP content increased from 35 wt% to 50 wt%, the *TS* of the ESA binder increased while the *EB* gradually decreased. Specifically, the *TS* increased from 2.56 MPa to 4.42 MPa, and the *EB* declined from 279% to 223%. As mentioned in the literature, an EP content of

35 wt% initially formed a cross-linked structure in the binder, and the structure was gradually enhanced with increasing EP content [25]. This contributed to the improvement of the mechanical properties of the ESA binder but compromised the toughness of the binder as the cross-linked structure would restrict the flow of the asphalt. In previous studies, the *TS* and *EB* of the EA50 binder were 3.6 MPa and 210%, respectively. Comparatively, the *TS* and *EB* of the ESA50 binder were elevated to 4.42 MPa and 223% [11,14]. The main reason was that the SBS-modified asphalt binder used in this study was obtained by the modification of the base binder, which had a better general performance. The Chinese specification (JTG/T 3364-02-2019) requires that $TS \geq 2$ MPa and $EB \geq 100\%$ for the performance of the EA binder for SBDP [24]. Undoubtedly, the tensile properties of all ESA binders could meet the requirements of engineering applications.

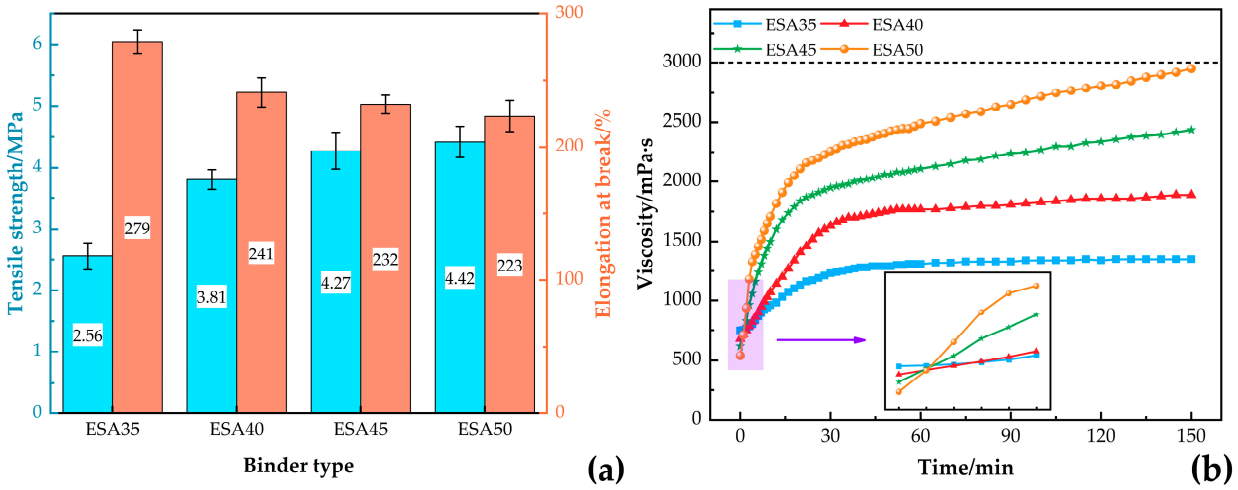

Figure 5. Test results of the ESA binder: (**a**) tensile test and (**b**) viscosity test.

The generation of curing reactions in ESA binders leads to an increase in viscosity. The ESA binder was generally required for a sufficient allowable time to ensure successful construction [37]. Figure 5b illustrates the viscosity test results of the ESA binder. It can be seen that, as the EP system viscosity was lower than that of SBS-modified asphalt binder at the same temperature, the initial viscosity of the ESA binder reduced with increasing EP content, from 748 mPa·s for ESA35 to 542 mPa·s for ESA50. Notably, the SBS-modified asphalt binder had a higher viscosity, such that the viscosity of the ESA binder was higher than that of the EA binder prepared with the base binder. Meanwhile, with the extension of the test time, the viscosity of the ESA binder exhibited a gradual increase, which was mainly attributed to the curing reaction happening, and the higher the EP content, the more substantial the reaction in the system, the faster the viscosity growth. After the test was conducted for 30 min, the change in the ESA binder viscosity slowed and displayed a linear change. At 150 min, the viscosities of ESA35, ESA40, ESA45, and ESA50 binders were 1350, 1890, 2440, and 2950 mPa·s, respectively. The Strategic Highway Research Program (SHRP) protocols stipulate that the asphalt binder viscosity should be ≤3000 mPa·s, and the allowable time should be ≥45 min. The results showed that the allowable time of all ESA binders could exceed 150 min, which satisfied the specification requirements.

5.2. High-Temperature Rutting Resistance

Compared with other geotechnical materials, the thermal conductivity of steel bridge plates is significantly higher, enabling the surface temperature of SBDP to often reach about 70 °C in summer [7]. Consequently, differing from the 60 °C used in the road pavement rutting test, the specification adopted the dynamic stability (*DS*) of 70 °C to constrain the high-temperature stability of the concrete, and the test results are shown in Figure 6.

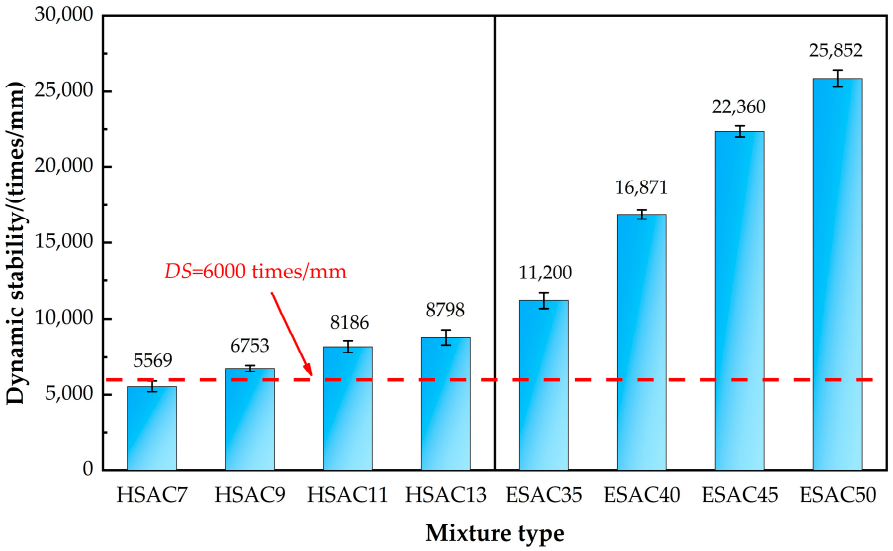

Figure 6. Rutting test results.

The results revealed that for HSAC, *DS* increased with rising TPS content, from 5569 times/mm for HSAC7 to 8798 times/mm for HSAC7. Adding TPS to the asphalt binder improved its viscosity, which helped to enhance the adherence between the asphalt and the aggregate, thus improving the high-temperature stability [28]. For ESAC, it can be seen that the *DS* of ESAC was significantly higher than that of HSAC, and even the minimum one, ESAC35, had a *DS* of 11,200 times/mm. It is indisputable that the ESA binder, as a thermosetting binder, resulted in concrete that had superior high-temperature performance. Additionally, the high-temperature stability of the concrete gradually enhanced with increasing EP content, and the *DS* of ESAC reached 25,852 times/mm. This is because, as demonstrated in the tensile tests, the higher the EP content, the more solid the cross-linked structure formed by the modifier, and the more outstanding the high-temperature performance of the asphalt concrete. The Chinese specification (JTG/T3364-02-2019) mentions the requirement of *DS* for asphalt concrete at 70 °C, which is ≥6000 times/mm [24]. As shown in Figure 6, except for HSAC7, the *DS* of other concretes can fulfill these requirements.

5.3. Low-Temperature Crack Resistance

Previous studies have shown that the crack is one of the most frequent defects of the SBDP in service, which is mainly due to the insufficient low-temperature crack resistance of the asphalt concrete [7]. As a result, it is necessary to focus on the low-temperature toughness of asphalt concrete. Figure 7 displays the beam bending test results for HSACs and ESACs.

TPS is a modifier that can visibly improve binder performance and has been investigated to support good elasticity to endow concrete with exceptional low-temperature performance [38]. The results in Figure 7 indicated that the ε_B of HSAC did not show an increasing or decreasing pattern with rising TPS content. ε_B of HSAC9 was the minimum, 3714 με, and ε_B of HSAC11 was the maximum, 4198 με. The specification (JTG/T3364-02-2019) requires the ε_B of asphalt concrete to be ≥3000 με [24]. The ε_B of HSAC was generally remarkably higher than the specification requirements, indicating that it had outstanding low-temperature crack resistance. Its use in the top layer of SBDP could dramatically reduce the occurrence of cracking defects and guarantee safe and comfortable driving conditions. In contrast, the ε_B of ESAC was apparently lower than that of HSAC, with ε_B of 3522, 3289, 3104, and 2836 με for ESAC35, ESAC40, ESAC45, and ESAC50, respectively. ε_B of ESAC had been improved compared with the results of previous studies due to the inherent good low-temperature toughness of SBS-modified asphalt binder. Simultaneously, it was evident that the ε_B of ESAC tended to decline continuously as the EP content increased, which was attributed to the cross-linked structural perfection in the ESA binder, which

restricted the flow of asphalt and negatively affected its toughness, corresponding to a continuous decrease in *EB* in the tensile test. Although ESAC was used for the bottom layer in this study, the concrete of the bottom layer was in direct contact with the steel bridge plate. It should have good synergistic deformation capability to prevent the cracking of the pavement top layer due to the occurrence of reflection cracks. Unfortunately, ESAC50 had the best high-temperature deformation resistance, but its low-temperature crack resistance failed to reach the requirements.

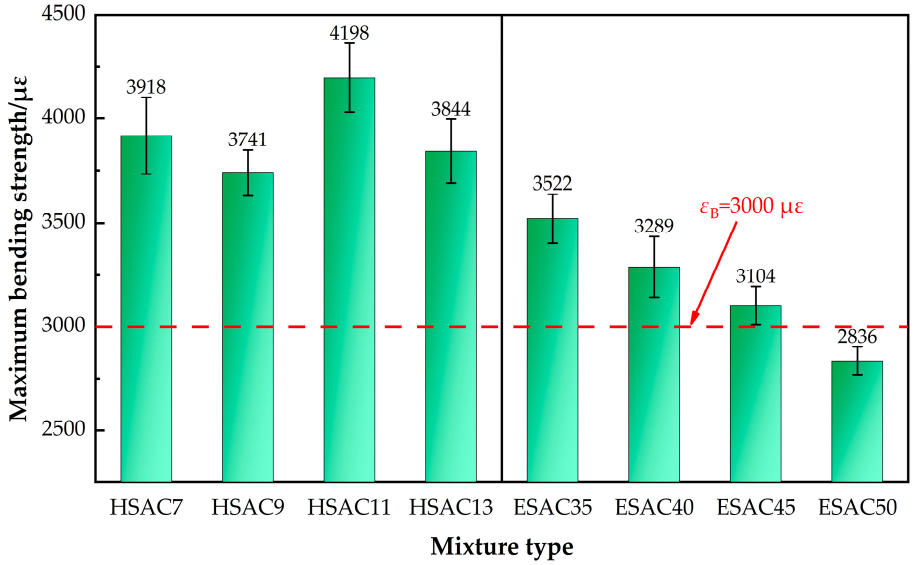

Figure 7. Beam bending test results.

5.4. Moisture Damage Resistance

Asphalt concrete in the service process is subject to temperature and precipitation, rainwater infiltration, and moisture in the concrete of the freezing and thawing cycles is prone to degradation of pavement performance, in severe cases, easily producing potholes, exfoliation, and other defects [39]. Hence, the moisture damage resistance of HSACs and ESACs was compared and evaluated. The test results are shown in Figure 8.

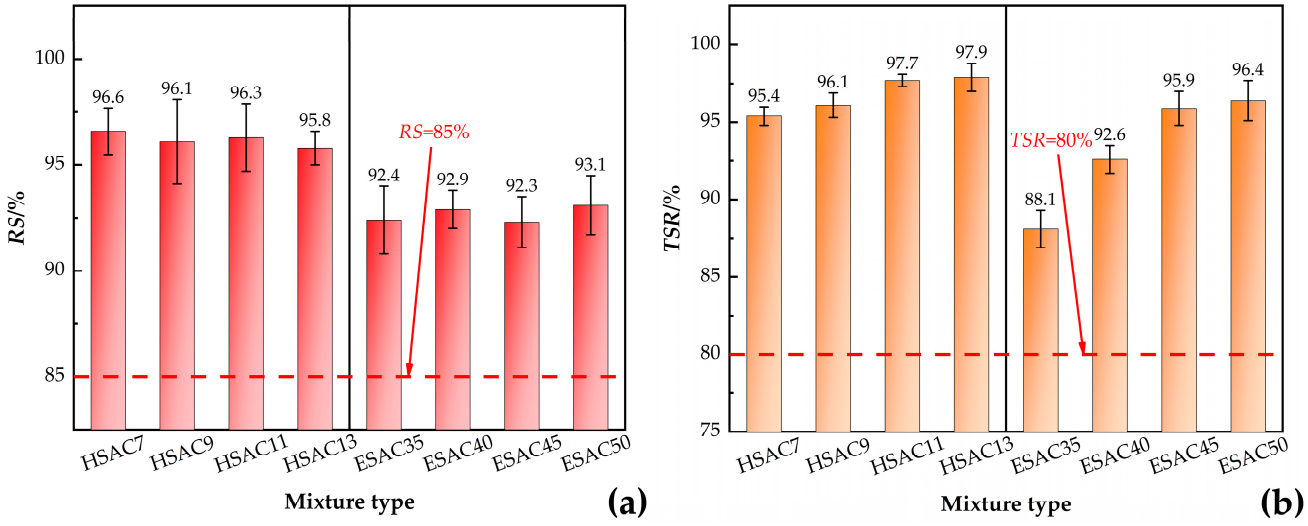

Figure 8. Moisture damage resistance test results: (**a**) Immersion Marshall test and (**b**) Freeze–thaw splitting test.

Both *RS* and *TSR* of the concrete in Figure 8 were below 100%, indicating that irreversible damage to the internal structure of the specimen occurred under the combined

effects of moisture and temperature, causing a deterioration in its stability and splitting strength. The water immersion Marshall test results demonstrated that the variation of TPS content did not influence the *RS* significantly. The *RS* of HSAC exceeded 95%, which was higher than the requirement of ≥85% in the specification (JTG/T3364-02-2019) [24]. Similarly, the *RS* of ESAC did not exhibit a monotonic variation with increasing EP content. The *RS* of ESAC35, ESAC40, ESAC45, and ESAC50 were 92.4%, 92.9%, 92.3%, and 93.1%, respectively, which were still much higher than 85%, although the test results were lower than the HSAC.

Conversely, the freeze–thaw splitting test results indicated that the variation of modifier content had a significant effect on the *TSR* of the concrete. Specifically, the *TSR* of both HSAC and ESAC gradually rose with increased modifier content. For HSAC, the addition of TPS dramatically improved the viscosity of the binder, enabling it to have superior adherence with the aggregate, effectively preventing the adverse effects of moisture, high temperature, low temperature, and other combined factors on the performance of concrete [40]. Meanwhile, the increase in TPS content caused the more evident improvement mentioned above. For ESAC, the enhancement of the cross-linked network structure within the binder positively affected the moisture damage resistance of the concrete, and the cohesion between asphalt and aggregate was strengthened with the increase in EP content [22]. Notably, the enhancement of *TSR* for HSMA13 and ESAC50 visibly slowed down compared to other concretes, with increasing values of 0.2% and 0.5%, respectively, suggesting that the excessive addition of modifiers was limited in improving the moisture damage resistance of concrete. The specification (JTG/T3364-02-2019) requires that the *TSR* of asphalt concrete should be ≥80% [24], and there is no doubt that all the concretes achieved this target. The results revealed that the moisture damage resistance of HSAC and ESAC was satisfactory, and HSAC was superior. Furthermore, it should be noted that the water immersion Marshall test was limited for evaluating the moisture damage resistance of concrete, and this test could not well-reflect the difference in performance between different concretes. Consequently, the freeze–thaw splitting test should be preferably chosen for the analysis of the moisture damage resistance.

5.5. Skid Resistance

The skid resistance of the pavement is directly related to the safety of vehicular traffic, and the pavement requires sufficient frictional resistance even in wet conditions [41]. Hence, it was crucial to conduct tests on the skid resistance of asphalt concrete. Figure 9 provides the results of the pendulum friction test.

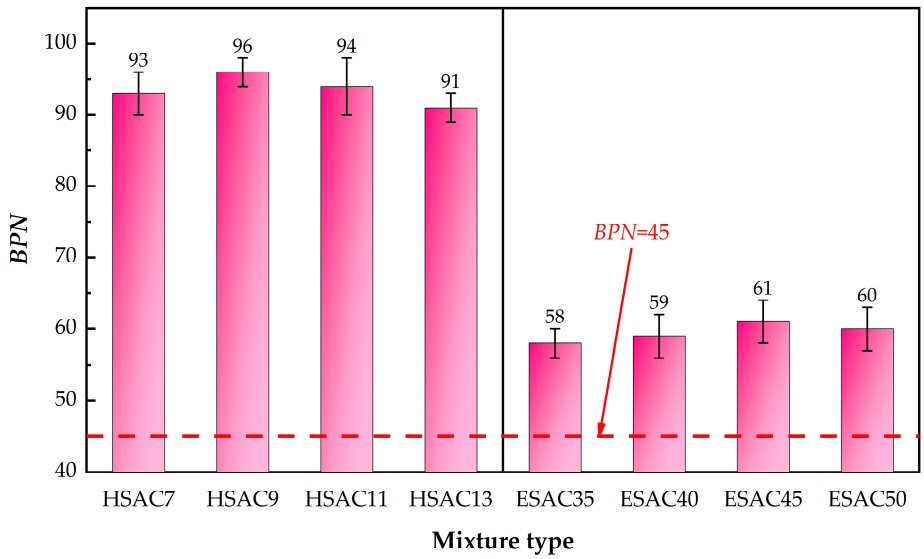

Figure 9. Skid resistance test results.

The variation of modifier content in the binder did not noticeably affect the skid resistance of HSACs and ESACs. The BPNs of HSACs were all above 90, exhibiting excellent skid resistance. In contrast, the BPN of ESAC was much lower, with BPNs of 58, 59, 61, and 60 for ESAC35, ESAC40, ESAC45, and ESAC50, respectively. On the one hand, compared to the dense graded EA-10, SMA-13 was a gap grading, and the proportion of coarse aggregate in HSAC was higher than that in ESAC, which could increase the pavement structure depth and thus its macroscopic texture was rougher; on the other hand, for the same gradation, the larger the nominal maximum aggregate size, the better the skid resistance of the concrete. As a result, the skid resistance of HSAC with SMA-13 grading was significantly better than that of ESAC with EA-10 grading. The Chinese specification (JTG 3450-2019) requires that the BPN of the pavement should be ≥45 [33], and the skid resistance of all HSACs and ESACs could meet the requirement. However, the aggregate on the pavement was subjected to the combined effects of friction, impact, and crushing of vehicle tires for a long time in the service process, which easily led to a continuous decline in skid resistance [42]. Thus, it is necessary to choose a gradation with superior initial skid resistance for the top layer to help enhance driving safety and extend the service life of the pavement, which is the crucial reason for using SMA-13 gradation in this project.

5.6. Service Performance of the Trial Section

According to the above performance tests of asphalt binders and concretes, it can be determined that the *DS* of HSAC7 and ε_B of ESAC50 failed to meet the specification requirements (JTG/T3364-02-2019) [24]. Although the *DS* and *TSR* of HSCA13 were ahead of HSAC11, the gap was not apparent. Meanwhile, the ε_B of HSAC11 was higher, which indicated that it had better low-temperature crack resistance. Furthermore, the increased EP content contributed to the improved high-temperature stability and moisture damage resistance of the concrete. Consequently, HSAC11 and ESAC45 were finally used for the pavement of the trial road. Currently, the pavement has been in operation for one year, and in order to comprehensively compare and understand the quality of the novel bridge deck pavement structure, a comprehensive inspection of its service condition was carried out. Before that, the traffic volume in different directions was enumerated. The results are shown in Figure 10.

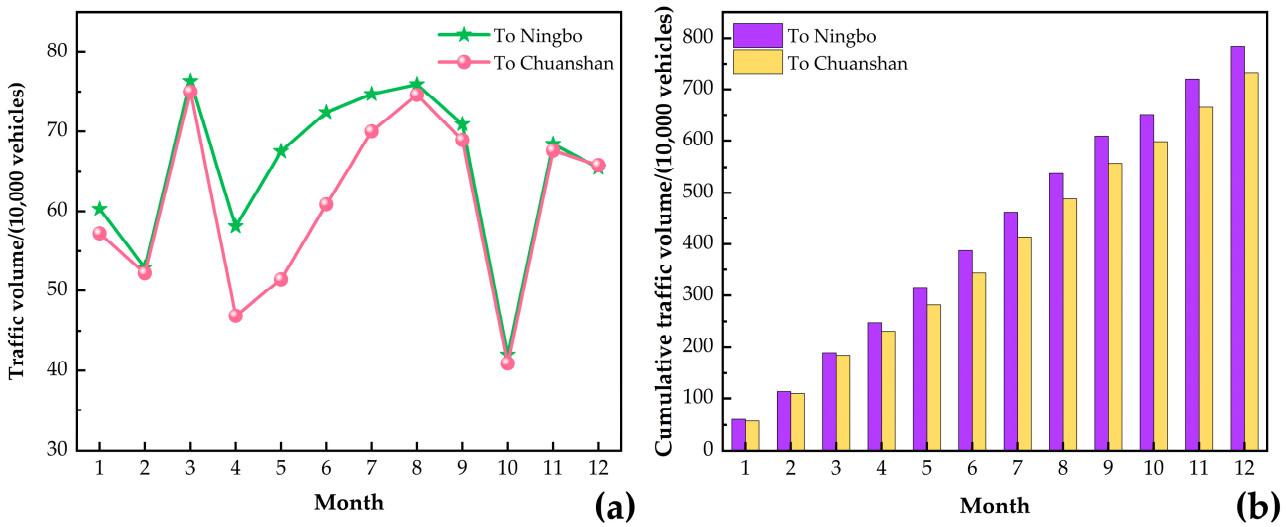

Figure 10. Traffic volume statistics: (**a**) single-month of traffic volume and (**b**) cumulative traffic volume.

From Figure 10a, it can be seen that the traffic volume of the trial road was highly variable over the months. For the lanes towards Ningbo, the highest monthly traffic volume appeared in March, with 763,000 vehicles; the lowest appeared in October, with 420,000 vehicles. For the lanes towards Chuanshan, the highest and lowest monthly traffic volumes also occurred in March and October, with 750,000 and 409,000 vehicles,

respectively. The main reason for this phenomenon is that the traffic control caused by COVID-19 led to a sharp drop in traffic volume during some periods. In general, the traffic volume in the lanes towards Ningbo was higher than that towards Chuanshan. Figure 10b shows the cumulative traffic volume of the two-way lanes. In 2022, the cumulative traffic volume of the lanes towards Ningbo was 7.849 million vehicles, and the cumulative traffic volume of the lanes towards Chuanshan was 6.8% lower compared to the Ningbo direction, which was 7.314 million vehicles.

The bridge deck pavement service conditions at K0008+700 to K0008+800 (right) and K0008+800 to K0008+900 (left) were thoroughly tested, and the results are shown in Figure 11.

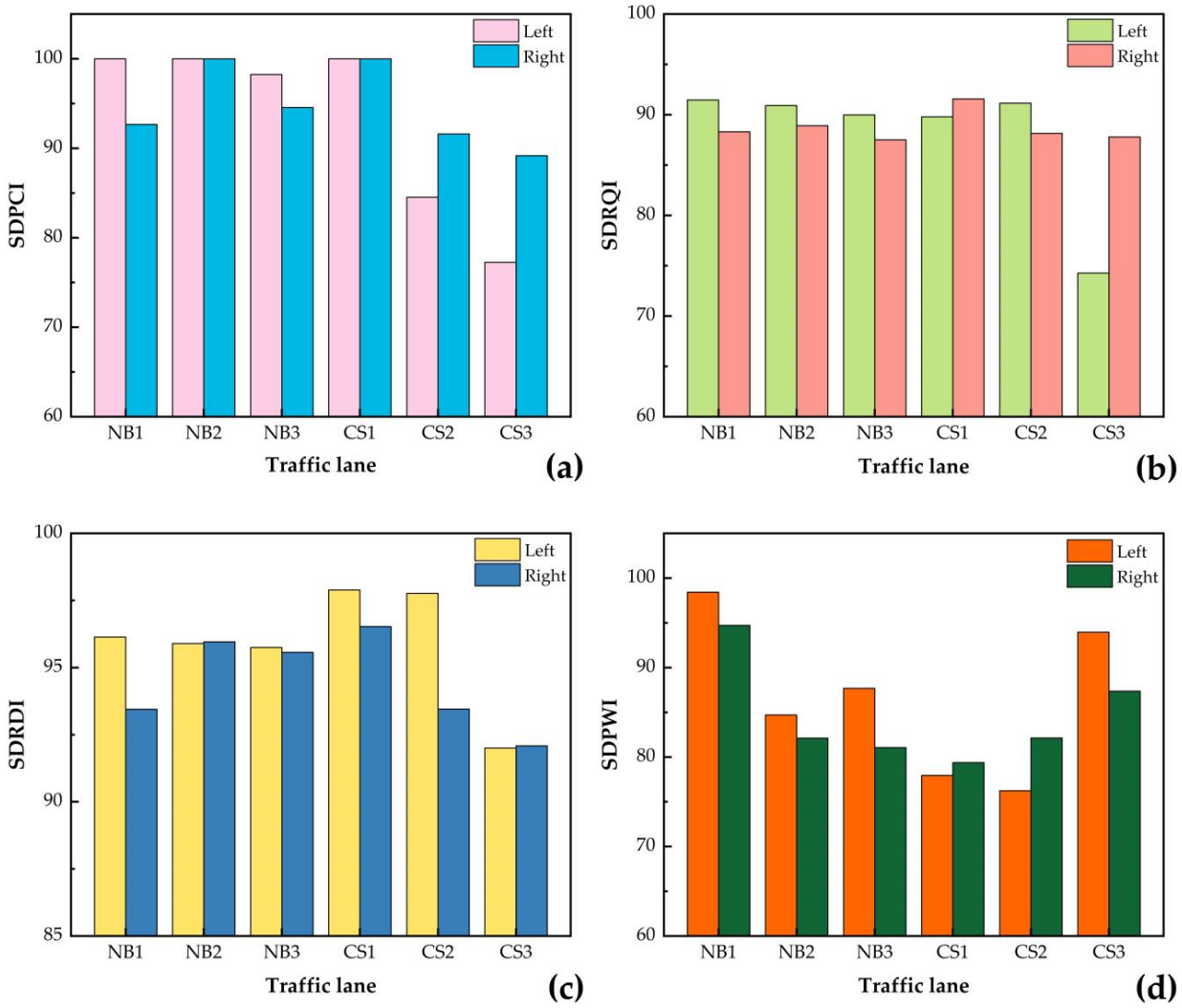

Figure 11. Bridge deck pavement evaluation results: (**a**) SDPCI, (**b**) SDRQI, (**c**) SDRDI, and (**d**) SDRWI.

SDPCI was used to reflect the damaged condition of the pavement, mainly including cracks, potholes, sinking, and loosening. The results in Figure 11a revealed that the SDPCI of some lanes reached 100, indicating that the surface of these lanes was basically devastation-free. The SDPCI of NB1, NB2, and NB3 lanes reached above 90. In contrast, the SDPCI of the right lanes of CS2 and CS3 were only 77.26 and 84.54, indicating that the pavement in the Chuanshan direction was significantly damaged. The reason for this may be the higher ratio of heavy load vehicles in lanes 2 and 3 compared to lane 1, leading to visible damage to the pavement in a short period, and also demonstrating that the bridge deck pavement constructed using the novel structure of SMAC + EAC had better resistance to defects.

The SDRQI quantifies the comfort of a vehicle driving through pavement flatness. As shown in Figure 11b, the gap in SDRQI was not apparent for all lanes except CS3, indicating that the whole driving quality of the bridge deck pavement was satisfactory. Notably, the SDRQI of the left lane of CS3 was significantly lower than that of the other lanes, only 74.28, which was similar to the results in the SDPCI and was mainly affected by the more severe defects existing in the pavement.

SDRDI was utilized to evaluate the pavement rutting damage degree. The results in Figure 11c revealed that the SDRDI reached above 90 for all lanes. Despite the different paving materials and structures used for the two directional lanes, the concrete had excellent high-temperature stability, which hindered the occurrence of pavement rutting distress to some extent. As a whole, the SDRDI of the NB lane was higher than that of the CS lane, especially the CS3 lane, which possessed the lowest SDRDI of 92.01 and 92.09.

SDPWI is used to assess the overall wearing rate of the pavement by measuring the texture depth at the wheel track zone. In the lane towards Ningbo, NB1 had the highest SDPWI with 98.43 and 94.72, and towards Chuanshan, CS3 had the highest SDPWI with 93.97 and 87.38. The results showed that the wear of the pavement was mainly concentrated in the NB2, NB3, CS1, and CS2 lanes, which meant that the skid resistance of these lanes was declining. It is worth noting that the overall SDPWI of the lane towards Ningbo was slightly higher than that of Chuanshan, probably because the top layer of the lane towards Ningbo used SMA-13 gradation. Its road surface roughness was higher than that of the lane towards Chuanshan using the SMA-10 gradation, which was relatively less adversely affected in the process of undergoing friction and impact of tires. Nevertheless, the whole abrasion resistance of the SBDP was unsatisfactory, which may be related to the quality of the aggregates. Consequently, it is necessary to use aggregates with a hard texture and superior abrasion resistance to prevent the rapid deterioration of pavement skid resistance in the initial service period [43].

The SDPQI of each lane was calculated using Equation (1). The results are shown in Figure 12. It can be seen that the SDPQI of each lane towards Ningbo was above 90, among which the right of NB3 lane was the lowest at 90.88; in contrast, the SDPQI of the lanes towards Chuanshan was significantly lower, except for the CS1 lane, which reached 93.80 and 94.32, and all other lanes were below 90. In particular, the SDPQI on the left of the CS3 lane was only 80.58. In order to visualize the service performance condition of each lane, it was divided according to the SDPQI value, as shown in Figure 13. Where $95 \leq$ SDPQI < 100 is Excellent, $90 \leq$ SDPQI < 95 is Good, $85 \leq$ SDPQI < 90 is Moderate, and $80 \leq$ SDPQI < 85 is Qualified.

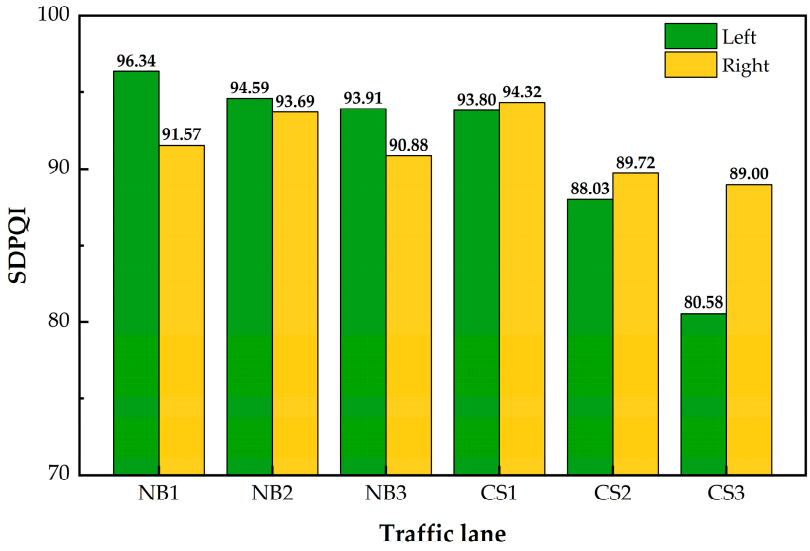

Figure 12. Results of SDPQI.

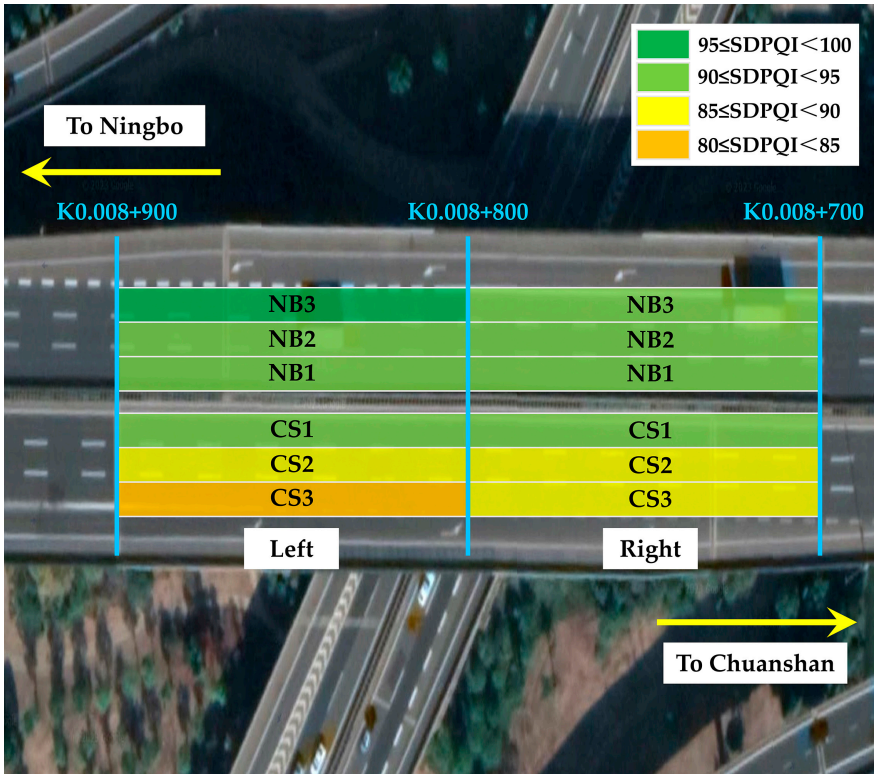

Figure 13. Service performance evaluation results for various lanes.

As shown in Figure 13, the SDPQI of all test lanes in the NB direction was above 90, with the SDPQI of the left of the NB3 lane reaching 96.34, and exhibiting excellent service performance. For the lanes towards Chuanshan, the CS1 lane performed favorably. However, the CS2 and CS3 lanes had poor pavement service performance, with the left CS3 lane only qualified and the other lanes performing moderately. It should be noted that the lanes near the centerline of the roadway, NB1 and CS1, are fast lanes with a high percentage of lightweight vehicles. In contrast, heavy vehicles generally travel in the NB2, NB3, CS2, and CS3 lanes. The pavement layer in the Chuanshan direction adopted the same ERS system as the old pavement structure, which was susceptible to defects such as rutting, cracks, and potholes under the action of heavy vehicles. On the contrary, although the annual traffic volume was higher in the NB direction, a novel pavement structure, SMAC + EAC, was used in this trial road. After indoor tests, both HSAC and ESAC used in the pavement have outstanding high-temperature rutting resistance and satisfactory low-temperature toughness, which can be well accommodated with the structural characteristics of steel bridge plates. This reduced the occurrence of rutting and cracking defects in the top layer as well as prevented reflection cracks caused by cracks in the bottom layer. Consequently, the novel pavement structure exhibited significantly improved service performance and lower performance degradation compared to the previous pavement solution. Even the NB2 and NB3 lanes, which have a high proportion of heavy vehicles, still performed well after one year of operation.

The successful application of the SMAC + EAC structure in the project provided favorable evidence for promoting this novel pavement structure in SBDP. This is extremely important for enhancing the service performance of SBDP, improving driving safety and comfort, as well as extending service life, which has outstanding economic and social benefits.

6. Conclusions

In this study, the tensile properties and viscosity characteristics of ESA binders with different EP contents were first analyzed by laboratory tests. Then, the pavement performance of ESAC and HSAC with different material compositions was investigated, and suitable asphalt mixtures were preferably selected for the trial road construction. Finally, the ERS system and SMAC + EAC structure were evaluated by combining the results of performance tests on the trial road in service for one year. The main conclusions can be summarized as follows:

(a) Using SBS-modified asphalt binder as the asphalt matrix helped to improve the strength and toughness of the ESA binder simultaneously. The increase in EP content enhanced the mechanical strength of the ESA binder but tended to affect the toughness negatively. Additionally, the construction allowable time for the ESA binder was sufficient and exceeded 150 min.

(b) ESAC and HSAC had good pavement performance; only the high-temperature performance of HSAC7 and the low-temperature performance of ESAC50 failed to meet the specification requirements. The optimal content of TPS in HAS binder and EP in the ESA binder were finally determined to be 11 wt% and 45 wt%, respectively.

(c) The ε_B and *BPN* of HSAC11 reached 4198 με and 94, and the outstanding low-temperature toughness and skid resistance contributed to the reduction of cracking disease in the top layer whilst improving the comfort and safety of driving. The DS of ESAC45 was 22,360 times/mm, and the excellent high-temperature stability and moisture damage resistance provided a stable pavement base for the top layer. Meanwhile, its satisfactory toughness synergized favorably with the steel plate, which limited the generation of cracks as well as reflective cracks in the bottom layer.

(d) The service condition of the trial road paved with the ERS system was inferior to that of the SMAC + EAC structure. The trial road paved with the ERS system only had one lane with an SDPQI above 90. In contrast, under the higher traffic volume, the SDPQI of all lanes of the trial road using the SMAC + EAC structure reached above 90. The excellent service performance of this novel steel deck pavement structure validated that its application is feasible and has the potential to be replicated.

(e) The service performance of the trial road will continue to be measured in the future to provide further data comparisons and analyses as a basis for promoting the SMAC + EAC structure.

Author Contributions: Conceptualization, Y.H. and H.G.; methodology, J.S.; software, Y.H.; validation, Y.H., H.G. and J.S.; formal analysis, Y.H.; investigation, J.S.; resources, H.G. and J.S.; data curation, J.S.; writing—original draft preparation, Y.H. and J.S.; writing—review and editing, H.G. and J.S.; visualization, J.S.; supervision, Y.H. and H.G.; project administration, H.G.; funding acquisition, H.G. All authors have read and agreed to the published version of the manuscript.

Funding: This research received no funding.

Institutional Review Board Statement: Not applicable.

Informed Consent Statement: Not applicable.

Data Availability Statement: All data, models, and code generated or used during the study appear in the submitted article.

Conflicts of Interest: No conflict of interest exists in the submission of this manuscript, and the manuscript is approved by all authors for publication. We would like to declare that the work described was original research that has not been published previously and was not under consideration for publication elsewhere, in whole or in part. All the authors listed have approved the manuscript that is enclosed.

Abbreviations

Abbreviations	Unit	Phrases
SBDP	/	Steel Bridge Deck Pavement
EAC	/	Epoxy Asphalt Concrete
GAC	/	Guss Asphalt Concrete
SMAC	/	Stone Mastic Asphalt Concrete
EA	/	Epoxy Asphalt
ECBL	/	Epoxy Bonding Chips Layer
RAC	/	Resin Asphalt Concrete
EP	/	Epoxy Resin
ESA	/	Epoxy SBS Asphalt
HSA	/	High-viscosity SBS Asphalt
TPS	/	TAFPACK-Super
ESAC	/	Epoxy SBS Asphalt Concrete
HSAC	/	High-viscosity SBS Asphalt Concrete
DS	times/mm	Dynamic Stability
ε_B	με	Maximum Flexural Strain
RS	%	Residual Stability
TSR	%	Tensile Strength Ratio
BPN	/	British Pendulum Number
TS	MPa	Tensile Strength
EB	%	Elongation at Break
SDPCI	/	SBDP Condition Index
SDRQI	/	SBDP Riding Quality Index
SDRDI	/	SBDP Rutting Depth Index
SDPWI	/	SBDP Wearing Index
SDPQI	/	SBDP Quality Index

References

1. Sun, J.; Zhang, Z.; Ye, J.; Liu, H.; Wei, Y.; Zhang, D.; Li, X. Preparation and properties of polyurethane/epoxy-resin modified asphalt binders and mixtures using a bio-based curing agent. *J. Clean. Prod.* **2022**, *380*, 135030. [CrossRef]
2. Heng, K.; Jia, P.; Xu, J.; Li, R.; Wu, H. Vehicular impact resistance of highway bridge with seismically-designed UHPC pier. *Eng. Struct.* **2022**, *252*, 113635. [CrossRef]
3. Shao, X.; Deng, L.; Cao, J. Innovative steel-UHPC composite bridge girders for long-span bridges. *Front. Struct. Civ. Eng.* **2019**, *13*, 981–989. [CrossRef]
4. Zhang, Z.; Sun, J.; Huang, Z.; Wang, F.; Jia, M.; Lv, W.; Ye, J. A laboratory study of epoxy/polyurethane modified asphalt binders and mixtures suitable for flexible bridge deck pavement. *Constr. Build. Mater.* **2021**, *274*, 122084. [CrossRef]
5. Liu, Y.; Qian, Z.; Hu, H.; Shi, X.; Chen, L. Developing a skid resistance prediction model for newly built pavement: Application to a case study of steel bridge deck pavement. *Road Mater. Pavement Des.* **2022**, *23*, 2334–2352. [CrossRef]
6. Jia, M.; Zhang, Z.; Yang, N.; Qi, B.; Wang, W.; Huang, Z.; Sun, J.; Luo, F.; Huang, T. Performance Evaluation of Thermosetting and Thermoplastic Polyurethane Asphalt Mixtures. *J. Mater. Civ. Eng.* **2022**, *34*, 04022097. [CrossRef]
7. Liu, Y.; Shen, Z.; Liu, J.; Chen, S.; Wang, J.; Wang, X. Advances in the application and research of steel bridge deck pavement. *Structures* **2022**, *45*, 1156–1174. [CrossRef]
8. Luo, S.; Qian, Z.; Yang, X.; Lu, Q. Laboratory Evaluation of Double-Layered Pavement Structures for Long-Span Steel Bridge Decks. *J. Mater. Civ. Eng.* **2018**, *30*, 04018111. [CrossRef]
9. Luo, S.; Lu, Q.; Qian, Z.; Wang, H.; Huang, Y. Laboratory investigation and numerical simulation of the rutting performance of double-layer surfacing structure for steel bridge decks. *Constr. Build. Mater.* **2017**, *144*, 178–187. [CrossRef]
10. Luo, S.; Qian, Z.; Yang, X.; Wang, H. Design of gussasphalt mixtures based on performance of gussasphalt binders, mastics and mixtures. *Constr. Build. Mater.* **2017**, *156*, 131–141. [CrossRef]
11. Luo, S.; Sun, J.; Hu, J.; Liu, S. Performance Evolution Mechanism of Hot-Mix Epoxy Asphalt Binder and Mixture Based on Component Characteristics. *J. Mater. Civ. Eng.* **2022**, *34*, 04022235. [CrossRef]
12. Zhang, D.; Ye, F.; Yuan, J. Analysis on Steel Bridge Pavement Structure Performance. *Procedia-Soc. Behav. Sci.* **2013**, *96*, 2462–2465. [CrossRef]
13. Chen, L.; Zhao, X.; Qian, Z.; Li, J. A systematic review of steel bridge deck pavement in China. *J. Road Eng.* **2023**, *3*, 1–15. [CrossRef]
14. Tian, J.; Luo, S.; Lu, Q.; Liu, S. Effects of Epoxy Resin Content on Properties of Hot Mixing Epoxy Asphalt Binders. *Journal of Mater. Civ. Eng.* **2022**, *34*, 04022145. [CrossRef]

15. Luo, S.; Liu, Z.; Yang, X.; Lu, Q.; Yin, J. Construction Technology of Warm and Hot Mix Epoxy Asphalt Paving for Long-Span Steel Bridge. *J. Constr. Eng. M* **2019**, *145*, 04019074. [CrossRef]
16. Fan, X.; Luo, R. Experimental study on crack resistance of typical steel-bridge-deck paving materials. *Constr. Build. Mater.* **2021**, *277*, 122315. [CrossRef]
17. Jia, X.; Huang, B.; Chen, S.; Shi, D. Comparative investigation into field performance of steel bridge deck asphalt overlay systems. *KSCE J. Civ. Eng.* **2016**, *20*, 2755–2764. [CrossRef]
18. Hu, D.; Lan, C.; Liang, N.; Wang, M.; Xiao, L. Prediction of Rutting Depth of Steel Bridge Deck Pavement Composite Structure Using Gussasphalt + SMA. *China J. Highw. Transp.* **2021**, *34*, 10–18. [CrossRef]
19. Liu, X.; Zhou, C.; Feng, D.; Fan, X.; Xie, S. Experimental study on interlayer shear properties of ERS pavement system for long-span steel bridges. *Constr. Build. Mater.* **2017**, *143*, 198–209. [CrossRef]
20. Liu, X.; Zhou, C.; Cao, Q.; Chen, L.; Feng, D. Experimental study on properties of epoxy binder and epoxy bonding chips layer for steel bridge deck pavement. *Road Mater. Pavement Des.* **2022**, *23*, 2451–2465. [CrossRef]
21. Chen, L.; Qian, Z.; Chen, D.; Wei, Y. Feasibility Evaluation of a Long-Life Asphalt Pavement for Steel Bridge Deck. *Adv. Civ. Eng.* **2020**, *2020*, 5890945. [CrossRef]
22. Sun, J.; Luo, S.; Huang, W.; Hu, J.; Liu, S. Structural optimization of steel bridge deck pavement based on mixture performance and mechanical simulation. *Constr. Build. Mater.* **2023**, *367*, 130217. [CrossRef]
23. *JTG F40-2004*; Technical Specification for Construction of Highway Asphalt Pavements. Ministry of Transport of China: Beijing, China, 2004.
24. *JTG/T3364-02-2019*; Specifications for Design and Construction of Pavement on Highway Steel Deck Bridge. Ministry of Transport of China: Beijing, China, 2019.
25. Sun, J.; Huang, W.; Lu, G.; Luo, S.; Li, Y. Investigation of the performance and micro-evolution mechanism of low-content thermosetting epoxy asphalt binder towards sustainable highway and bridge decks paving. *J. Clean. Prod.* **2023**, *384*, 135588. [CrossRef]
26. Xie, H.; Li, C.; Wang, Q. A critical review on performance and phase separation of thermosetting epoxy asphalt binders and bond coats. *Constr. Build. Mater.* **2022**, *326*, 126792. [CrossRef]
27. Gong, J.; Liu, Y.; Wang, Q.; Xi, Z.; Cai, J.; Ding, G.; Xie, H. Performance evaluation of warm mix asphalt additive modified epoxy asphalt rubbers. *Constr. Build. Mater.* **2019**, *204*, 288–295. [CrossRef]
28. Zhang, Z.; Chen, L.; Peng, J.; Sun, J.; Zhang, D.; Li, X.; Wen, F.; Liu, H. Preparation and properties of a novel high-viscosity modified bitumen. *Constr. Build. Mater.* **2022**, *344*, 128183. [CrossRef]
29. Kiselev, A.; Zhang, H.; Liu, Z. The effect of two-phase mixing on the functional and mechanical properties of TPS/SBS-modified porous asphalt concrete. *Constr. Build. Mater.* **2021**, *270*, 121841. [CrossRef]
30. Jiao, Y.; Zhang, Y.; Fu, L.; Guo, M.; Zhang, L. Influence of crumb rubber and tafpack super on performances of SBS modified porous asphalt mixtures. *Road Mater. Pavement Des.* **2019**, *20*, S196–S216. [CrossRef]
31. *ASTM D638-14*; Standard Test Method for Tensile Properties of Plastics. ASTM International: West Conshohocken, PA, USA, 2014.
32. *ASTM D4402*; Standard Test Method for Viscosity Determination of Asphalt at Elevated Temperatures Using a Rotational Viscometer. ASTM International: West Conshohocken, PA, USA, 2015.
33. *JTG E60-2019*; Field Test Methods of Highway Subgrade and Pavement. Ministry of Transport of China: Beijing, China, 2019.
34. *JTG E20-2011*; Highway Engineering Asphalt and Asphalt Mixture Test Regulations. Ministry of Transport of China: Beijing, China, 2011.
35. *JTG 5210-2018*; Highway Performance Assessment Standards. Ministry of Transport of China: Beijing, China, 2018.
36. *JTG 5210-2018*; Technical Specification for Maintenance Technology of Long Span Bridge Steel Deck Epoxy Asphalt Concrete Pavement. Jiangsu Provincial Bureau of Quality and Technical Supervision: Nanjing, China, 2017.
37. Sun, J.; Zhang, Z.; Wang, L.; Liu, H.; Ban, X.; Ye, J. Investigation on the epoxy/polyurethane modified asphalt binder cured with bio-based curing agent: Properties and optimization. *Constr. Build. Mater.* **2022**, *320*, 126221. [CrossRef]
38. Zhong, K.; Sun, M.; Chang, R. Performance evaluation of high-elastic/salt-storage asphalt mixture modified with Mafilon and rubber particles. *Constr. Build. Mater.* **2018**, *193*, 153–161. [CrossRef]
39. Jia, M.; Sha, A.; Jiang, W.; Li, X.; Jiao, W. Developing a solid–solid phase change heat storage asphalt pavement material and its application as functional filler for cooling asphalt pavement. *Energy Build.* **2023**, *285*, 112935. [CrossRef]
40. Huang, S.C. Rubber Concentrations on Rheology of Aged Asphalt Binders. *J. Mater. Civ. Eng.* **2008**, *20*, 221–229. [CrossRef]
41. Fwa, T.F. Skid resistance determination for pavement management and wet-weather road safety. *Int. J. Transp. Sci. Technol.* **2017**, *6*, 217–227. [CrossRef]
42. Yu, Y.; Tang, S.; Xu, G.; Fan, Y.; Wu, Y.; Wang, H.; Yang, J. Investigations on the long-term skid resistance of epoxy asphalt mixture based on accelerated loading test. *Constr. Build. Mater.* **2023**, *365*, 130150. [CrossRef]
43. Zeng, G.; Xu, W.; Huang, H.; Zhang, X. Study on the microstructure and properties of hot-mix epoxy asphalt. *Int. J. Pavement Res. Technol.* **2019**, *12*, 147–153. [CrossRef]